Magnonic Hong-Ou-Mandel effect

Mikhail Kostylev ®*

Department of Physics, University of Western Australia, Crawley, 6009 Western Australia, Australia

We carried out numerical simulations of propagation of spin waves (magnons in quantum language) in an yttrium-iron garnet film. The numerical model is based on an original formalism. We demonstrated that a potential barrier for magnons, created by an Oersted field of a dc current flowing through a wire sitting on top of the film, can act as an electrically controlled partly transparent mirror for the magnons. We found that the mirror transparency can be set to 50% by properly adjusting the current strength, thus creating a semitransparent mirror. A strong Hong-Ou-Mandel effect for single magnons is expected in this configuration. The effect must be seen as two single magnons, launched simultaneously into the film from two transducers located from the opposite sides of the mirror, creating a two-microwave-photon state at the output port of one of the transducers. The probability of seeing those two-photon states at the output port of either transducer must be the same for both transducers.

I. INTRODUCTION

The Hong-Ou-Mandel effect (HOME) represents a particular manifestation of the property of indistinguishable bosonic particles to bunch. It has been studied in detail for optical photons and is seen as a specific interference pattern which is generated by pairs of photons while incident on a 50:50 lossless optical beam splitter [1]. If two indistinguishable optical photons are simultaneously incident on the beam splitter, each onto its own input port, both of them always exit the splitter together through the same output port but never separately with one photon through each of the two output ports [2,3]. Later, it was theoretically shown that, if the beam splitter is lossy, the same interference pattern must remain for coincidence photons, i.e., when both photons survive the transmission through the lossy medium.

Very recently, the same effect was demonstrated in quantum acoustics for pairs of traveling phonons. Surface acoustic waves (SAWs) in LiNbO$_3$ plates were employed to observe this effect [4]. In this paper, we make a theoretical prediction that the same effect can be seen for traveling microwave magnons in single-crystal yttrium iron garnet (YIG) films. Central for observation of HOME is the availability of a semitransparent mirror for specific (quasi-)particles, for which the effect is to be observed. In this paper, we propose a partly transparent mirror for magnons, the degree of transparency of which can be controlled electrically; investigate its properties theoretically; and consider its usefulness for observing HOME for traveling magnons. Importantly, we do this specifically for short spin-wave (SW) pulses. The reason for that will be explained below.

Magnons (or magnon-polaritons) are bosonic quasiparticles that represent quanta of SWs. Quantum magnonics has attracted a lot of attention recently; see Ref. [5] for a recent review on that matter and references therein. For instance, excitation and propagation of SWs at millikelvin temperatures was successfully demonstrated [6,7], It has also been shown that traveling single magnons can be employed to convert microwave photons to optical photons [8] and that parametrically squeezed states of traveling magnons can be created [9]. Classically, SWs represent collective precession of electron spins in a magnetic material. The collective character of the spin dynamics is due to coupling of spins at nearby crystal lattice sites by exchange and dipole-dipole interactions. The best medium for experiments with traveling magnons is thin single-crystal films of YIG. In these films and for small magnon wave numbers k (0 to 1000 rad/cm), the coupling of ferromagnetic spins is predominantly by a dynamic dipole (or stray) magnetic field they generate collectively while precessing. The total magnon energy is then the sum of energies of the dipole-dipole and Zeeman interactions. The Zeeman interaction results in formation of an energy gap in the magnon spectrum, such that application of a reasonably small external spatially uniform magnetic field H able to saturate the YIG films magnetically shifts the frequency of SWs $\omega(k = 0)$ into the microwave frequency range.

In addition, the dependence of SW dispersion $\omega(k)$ on the applied field results in efficient scattering of traveling SWs from localized nonuniformities of a magnetic field applied to a YIG film [10,11]. A field nonuniformity can easily be created by placing a narrow metallic wire on top of the film and sending a relatively small dc current through it. The current induces a dc Oersted field around the wire. The Oerstead field is highly localized, thus forming the necessary conditions for efficient SW scattering from the Zeemann energy barrier.

In Ref. [11], it was shown that, by controlling the strength of the current, the coefficients of SW transmission and reflection from the localized nonuniformity may be varied in a very broad range—from complete reflection to complete transmission. This potentially creates conditions for forming a semitransparent mirror for magnons traveling in the film.

*mikhail.kostylev@uwa.edu.au

Importantly, the SW dispersion strongly depends on the orientation of the applied field with respect to the film surface and the direction of SW propagation in the film plane [12,13]. To use the Oerstead field of a wire as a narrow energy barrier, the wire must lie in the film plane, be orientated perpendicular to the SW wave vector, and have a component of its Oersted field parallel to a static spatially uniform magnetic field also applied to the film. These conditions are satisfied for the backward volume magnetostatic SW (BVMSW) and the forward volume magnetostatic SW (FVMSW). A FVMSW propagates in a film which is magnetized by applying a static field perpendicular to its plane [13]. A wave has a BVMSW character if a film is magnetized in its plane and the wave propagates along the direction of the applied field [12].

In this paper, we focus on creating an electrically controlled mirror for BVMSWs. The case of FVMSWs is slightly more involved, as these waves scatter from the perpendicular-to-plane component of the Oersted field of a wire. This component of the field has an antisymmetric shape in the direction of the SW wave vector. This breaks symmetry of the scattering geometry. Our numerical simulation shows that the symmetry break results in slightly different time delays of waves reflected from the barrier if they are incident onto the barrier from its opposite sides. This may affect indistinguishability of single magnons scattered from the mirror.

On the contrary, BVMSWs are sensitive to the component of the wire Oersted field that lies in the film plane. This component is symmetric and hence must preserve indistinguishability of magnons. It is the main reason for the focus on BVMSWs in this paper, and we do not consider FVMSWs any further.

It is important to emphasize the difference of the present treatment of the effect of BVMSW scattering from the potential barrier created by the Oersted field of a dc current in a wire from the earlier work [11]. The theory of SW scattering from Ref. [11] lacks time dependence. As a result, the integral equation obtained in that earlier work is suitable for modeling continuous-wave (CW) or single-frequency SW signals. However, as follows from Ref. [4], the single-microwave-photon output of superconducting qubits represents a radiofrequency (RF) pulse of ~ 20 ns in duration.

The SAW phonons are dispersionless, meaning that the dispersion law $\omega(k)$ for them represents a straight line. (Here ω is the wave frequency and k is its wave number.) This is an important difference between Ref. [4] and this paper. SWs in thin magnetic films are fundamentally dispersive—the dependence $\omega(k)$ for them is not a straight line. This implies that SW group velocity $V_g = d\omega/dk$ is k dependent. As a result, different parts of the frequency spectrum of an RF pulse carried by SWs travel with different speeds. This leads to dispersive broadening of the pulse both in space and time, potentially severely deforming the pulse shape. The adverse impact of the dispersion increases with a decrease in the SW pulse length. For YIG films with thicknesses typically used in SW experiments (5–7 μm), the dispersion spreading becomes significant for pulse lengths < 25ns or so (see, e.g., Ref. [14]). Shaping the microwave photons released by the superconducting qubits as 17-ns-long pulses, as was done in Ref. [4], thus requires considering SW dynamics time resolved.

In addition, in Ref. [11], it was shown that the efficiency of scattering of a CW SW from a potential barrier created by a dc current in a wire is strongly k dependent. This suggests that the shape of a SW waveform of a nonvanishing spectral width may be noticeably modified during the process of scattering from the potential barrier. Furthermore, due to the presence of the energy gap in the SW spectrum (which also distinguishes magnons from SAW phonons), it is important to ensure that the whole spectral width of input microwave pulses that excite the traveling SW pulses fits into the allowed energy band for magnons [14]. If it does not, spectral components of the RF pulse that fall into the energy gap will get filtered out. This will contribute to a further distortion of the temporal/spatial shape of the SW pulse. Modeling the SW dynamics time resolved is the direct way to account for these two effects too.

All these aspects call for considering the process of SW scattering from the energy barrier time resolved and specifically for short SW pulses. Accordingly, in this paper, we derive an integrodifferential equation that governs classical dynamics of the envelopes of narrow packets of BVMSWs in a ferromagnetic film and simulate excitation, propagation, and scattering of SWs by numerically solving the envelope equation.

We show that short BVMSW pulses scatter efficiently from a Zeemann energy barrier created by an Oersted field of a dc current in a wire orientated in the film plane and along the BVMSW fronts. If parameters of the physical process are properly selected, the pulses are not significantly affected by the dispersive character of BVMSWs and the k-dependent efficiency of SW scattering from the barrier. By properly adjusting the current through the wire, a semitransparent SW mirror can be created. The mirror is characterized by a transfer matrix that satisfies requirements for the presence of a HOME for it. We also discuss technical details of how to organize a future experiment on observation of the magnonic HOME based on the proposed semitransparent SW mirror.

The paper is organized as follows. Section II presents the developed time-resolved theoretical model and results of numerical simulations of scattering of BVMSW pulses from the energy barrier. Section III introduces details the SW HOME, which follow from the numerical simulations, and discusses technical details of the proposed SW HOME experiment. Section IV contains conclusions. Technical details of the derivation of the model equation, the numerical solution of the equation, and less important results of the numerical simulation are placed in the appendices.

II. THEORY AND SIMULATION RESULTS

Figure 1 shows a sketch of the problem geometry. Its main component is a 5-μm-thick ferromagnetic film (film thickness $L = 5$ μm). The film is magnetized in its plane by a spatially uniform magnetic field **H** of a strength $\mu_0 H = 85$ mT ($H = 850$ Oe). Two wire-loop transducers (labeled ports 1 and 2) are placed $d = 7$ mm apart and perpendicular to the applied field. This creates conditions for the excitation of BVMSWs in the film. The transducers are also used to receive the signals carried by BVMSWs. Appendix C explains why we opt for the loop transducers in our simulations and how we simulate the driving microwave magnetic field h_{dr} of a transducer operating
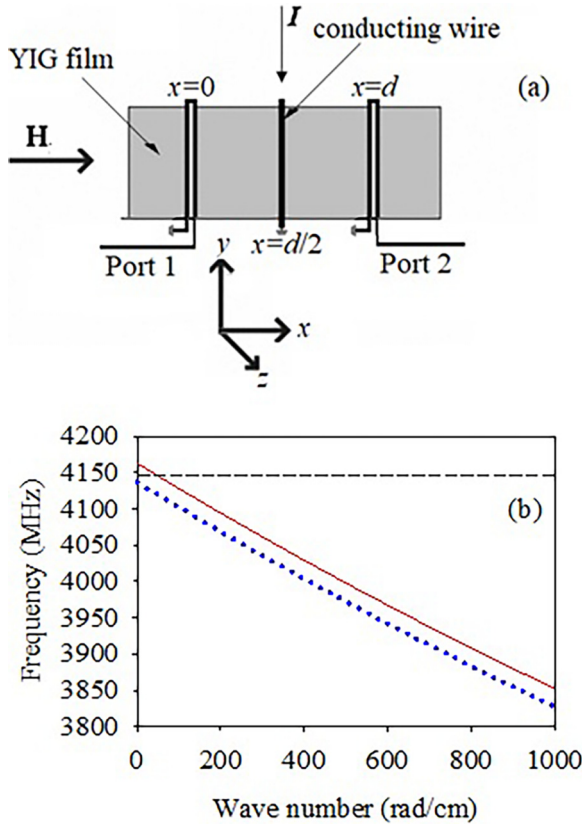
FIG. 1. (a) Sketch of the simulated geometry. (b) Backward volume magnetostatic spin wave (BVMSW) dispersion for a 5-μm-thick yttrium iron garnet (YIG) film. Solid line: applied field $H = 850$ Oe. Dotted line: a slightly smaller applied field $H = 842$ Oe. Thin dashed line shows the carrier frequency of the simulated input microwave pulses $\omega_0/2\pi = 4145$ MHz.
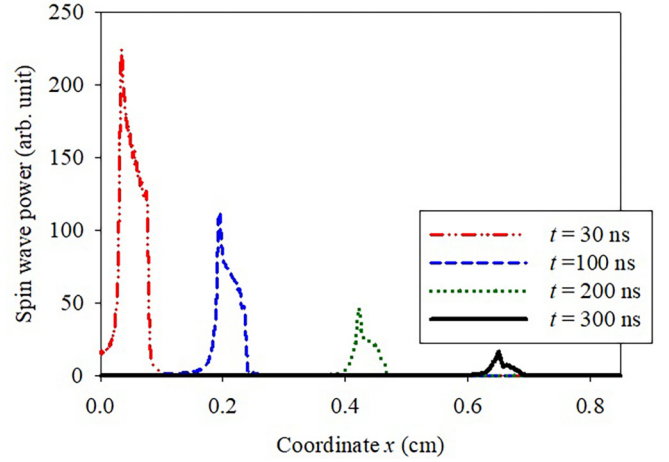

FIG. 2. Snapshots of backward volume magnetostatic spin wave (BVMSW) pulses taken at different moments of time t (see the legend). Carrier wave number of pulses is 49 rad/cm, which corresponds to $\omega_0/2\pi = 4145$ MHz. Applied field $H = 850$ Oe. Film thickness $L = 5$ μm. Length of input microwave pulses: 20 ns. The pulses are excited by the transducer located at $x = 0$. No potential barrier is present ($I = 0$).

as an input one and how we simulate output transducer signals when a transducer receives a BVMSW signal.

A single wire (shown as "conducting wire" in the sketch) is located midway between the transducers (i.e., at $x = d/2 = 3.5$ mm). The wire width $\omega = 50$ μm. The wire carries a dc current I. The Oersted field of the current $\delta h(I,x)$ creates a potential barrier for SWs in the film. A BVMSW pulse is excited by one transducer, or two counterpropagating SW pulses are excited by both transducers simultaneously. The SW pulse(s) travel(s) through the film and scatter(s) from the barrier to create reflected and transmitted pulse(s). The reflected and transmitted pulses are received by the transducers and create output microwave signals of ports 1 and 2.

As shown in Appendix A, the BVMSW dynamics in this geometry is governed by an integrodifferential equation as follows:

$$\frac{dm(x,t)}{dt} - i\left\{\frac{[\omega_H + \gamma\,\delta h(I,x)]^2}{2\omega_0} - \frac{\omega_0}{2}\right\}m(x,t)$$

$$+ i\frac{[\omega_H + \gamma\,\delta h(x)]\omega_M}{2\omega_0}\int_{-\infty}^{\infty}\hat{G}(x - x')m(x',t)dx'$$

$$= -i\frac{\omega_H\omega_M}{2\omega_0}h_{\mathrm{dr}}(x,t). \tag{1}$$

Here, γ is the gyromagnetic ratio, which is equal to $2\pi \times 28$ MHz/mT ($2\pi \times 2.8$ MHz/Oe) for YIG, $\omega_H = \gamma(H + i\Delta H)$, $2\Delta H = 0.5$ Oe is the magnetic loss parameter for YIG (at room temperature), i is imaginary unit, $\omega_M = \gamma\mu_0 M$, where μ_0 is permeability of vacuum, M is the saturation magnetization of the films ($\mu_0 M = 175$ mT for YIG), and $m(x, t)$ and $h_{\mathrm{dr}}(x, t)$ are the perpendicular-to-film-plane vector components of the slow envelopes of dynamic magnetization of BVMSWs and of the microwave driving field, respectively. They are slow with respect to the microwave carrier frequency ω_0 of these waveforms. The expressions for the Green's function of the perpendicular-to-plane component of the dipole magnetic field of the dynamic magnetization $\hat{G}(s)$ [15] and for the in-plane component of the Oersted field $\delta h(I,x)$ of the wire that creates the potential barrier are given in Appendixes A and B, respectively.

In this paper, we solve the envelope equation numerically. We use a mesh of 1000 discrete coordinate points $x = x_n$, $n = 1, 2, \ldots, 1000$. This creates a 1000-component vector with components $m(x_n, t)$. We employ the fourth-order Runge-Kutta method to obtain a time-dependent solution for the vector. The whole solution process is implemented as a MathCAD worksheet employing MathCAD's Adaptive Runge-Kutta solution function Rkadapt. Simulating the whole process of pulse scattering from the barrier takes 3–5 min of computer time.

Like the experiment on the phononic HOME [4], we assume that microwave superconducting qubits act as sources of single microwave photons, which the transducers convert into single magnons. The photons were formed as 17.6-ns-long pulses in Ref. [4]. Similarly, we use 20-ns-long rectangular-shaped pulses as $h_{\mathrm{dr}}(t)$.

All simulations in this paper are carried out for a carrier wave number of SWs of 49 rad/cm. This corresponds to $\omega_0 = 4145$ MHz, as shown in Fig. 1(b). Figure 2 displays

the simulated screenshots of a BVMSW pulse launched by the transducer located at $x = 0$ (Port 1). The screenshots are taken at different moments of time t. No potential barrier is present ($I = 0$). Here, $t = 0$ corresponds to the front edge of the driving pulse $h_{dr}(t)$. The transducer excites two BVMSW pulses traveling in two opposite directions from it, but we only show the pulse propagating toward the receiving antenna (located at $x = 7$ mm).

The waveform shape evolves during the pulse propagation in the film. The shape of the envelope of the BVMSW pulse is not rectangular even for small t. This is because the pulse edges are smoothed during the transduction process due to the finite width of the transduction frequency/wave number band of the transducer. As the pulse propagates in the film, it broadens and its height drops. The former is an effect of the presence of dispersion, which distinguishes SW pulses from SAWs exploited in Ref. [4]. The dispersion law for the fundamental mode of BVMSWs is shown in Fig. 1(b). One sees that the eigenfrequency vs wave number dependence for the waves does not represent a straight line—the line has a slight positive curvature. This makes narrow pulses carried by BVMSWs prone to dispersion broadening [16].

The decrease in the pulse amplitude has two origins. The first one is the presence of magnetic loss in the medium. Due to the loss, the pulse amplitude drops exponentially with distance from the location of pulse excitation. The second origin is the conservation of pulse energy—when a pulse broadens in a dispersive medium, its height must decrease to conserve energy of the pulse.

Figure 3(a) demonstrates exemplary snapshots of the same BVMSW pulse taken in the presence of a potential barrier. Here, $I = -0.35$ A for the example. The negative sign indicates that, within the film, the Oersted field of the current is antialigned to the applied field **H**. As a result, the total static field within the barrier is smaller than elsewhere. This regime of SW transmission through a barrier was termed *tunneling* in Refs. [10,11]. The decrease in the total static field locally shifts the dispersion relation downward in frequency. If the shift is small, this just makes the local value of the BVMSW wave number smaller. However, for larger magnitudes of the negative I, the downshift of the dispersion relation becomes large enough to place the BVMSW frequency locally into the energy gap that exists above the BVMSW band. This situation is shown in Fig. 1(b) by the dotted line. One sees that, for a smaller H, any point of the dispersion relation lies below ω_0 (shown by the horizontal dashed line). Then the only way for a BVMSW to cross the barrier is by tunneling through it as a leaky wave.

The example from Fig. 3(a) is for a specific value of I, for which energy of the transmitted (the right-hand-side waveform) pulse equals to energy of the reflected pulse (the left-hand-side pulse). The quantity we plot in the graph is $|m(x, t)|^2$. Power carried by a SW must scale as $|m(x, t)|^2$. Therefore, in the following, we term this quantity *SW power*. Similarly, integrating $|m(x, t)|^2$ over the spatial or temporal width of the pulse, we obtain a quantity which scales as pulse energy. In the following, we will term the integral *pulse energy*.

In Fig. 3(a), the barrier is located at $x = 0.35$ cm. One sees that the scattered pulses are located at equal distances from
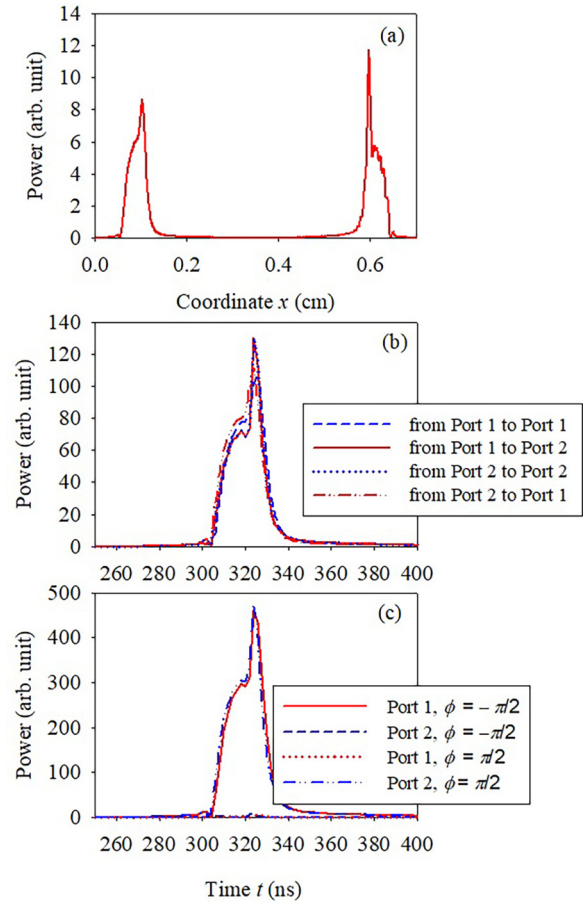

FIG. 3. (a) Snapshot of backward volume magnetostatic spin wave (BVMSW) pulses scattered from a barrier $I = -0.35$ A. The snapshot corresponds to $t = 140$ ns. (b) Output microwave signals of Port 1 (denoted as "to Port 1" in the legend) and Port 2 (denoted as "to Port 2"), when a single input microwave pulse is applied to either Port 1 (denoted as "from Port 1") or Port 2 (denoted as "from Port 2"). The barrier height is the same as for (a). (c) The same as (b), but the same microwave pulses are now applied to both ports simultaneously. Ports 1 and 2 in the legend denote the ports that receive the respective signals. ϕ is the initial phase of the input microwave pulse applied to Port 2. The initial phase of the input pulse fed into Port 1 is zero. The barrier height is the same ($I = -0.35$ A). The other simulation parameters are the same as for Fig. 2.

this point. This demonstrates that the pulses acquire the same time delay while scattering from the barrier. This is better seen from Fig. 3(b), which displays microwave signals received by the transducers. The signal from Port 1 is the reflected signal, and the one exiting Port 2 is the transmitted one. One sees that the shapes of the output pulses are slightly different, but they overlap quite well in time. The same power vs t traces are obtained when we excite an SW pulse with the second transducer (Port 2) located at $x = 0.7$ cm. The only difference is that the reflected pulse is now received by Port 2 and the transmitted one by Port 1.

Panel (c) of the same figure displays the output pulses of the ports for a case when two identical rectangular microwave pulses are applied to both ports simultaneously. The only difference between the input pulses is their initial phases. The

phase difference between the input pulses is either $+\pi/2$ or $-\pi/2$. We see that, in either case, the microwave signal from one port is strong, and the output signal of the other port is strongly suppressed. This behavior is in full agreement with what is expected from an optical semitransparent mirror [2]. We also see that changing the phase difference by π (i.e., from $+\pi/2$ to $-\pi/2$) swaps ports, through which the larger and smaller pulses exit. Again, this agrees with what is expected from an optical semitransparent mirror [17].

Figure 3(c) is the main finding of this paper. It demonstrates that the barrier acts as semitransparent mirror for short SW pulses, for which we may expect a magnonic HOME. However, before we proceed to a discussion of the effect, it is worth noting that the mirror transparency is electrically controlled. The ratio R of transmitted and reflected pulse energies can easily be decreased or increased by altering I. This is shown in Appendix D.

III. MAGNONIC HOME

Important for a theoretical description of HOME is establishing the transfer matrix for a semitransparent mirror. The general form of the matrix is

$$\hat{S} = \begin{pmatrix} S_{11} & S_{12} \\ S_{21} & S_{22} \end{pmatrix}. \qquad (2)$$

The matrix element S_{11} represents the signal exiting Port 1 if an input pulse of amplitude of 1 is applied to Port 1. Similarly, S_{22} is the output signal of Port 2 if an input pulse is applied to Port 2. Physically, these quantities represent reflection coefficients from the barrier. Here, S_{21} and S_{12} represent the coefficients of transmission of the mirror—from Port 1 to Port 2 and from Port 2 to Port 1, respectively. All these quantities are complex valued. A BVMSW is a reciprocal wave (i.e., it has the same properties while propagating in $+x$ and $-x$ directions); therefore, we expect that $S_{22} = S_{11} = \tau$ and $S_{12} = S_{21} = r$, where we introduced the complex-valued transmission τ and reflection r coefficients. Our numerical simulation results are in excellent agreement with these equalities.

We will establish the matrix specifically for the case of a perfectly semitransparent mirror and for the pulse regime we studied above. This implies that energy of the transmitter pulse equals energy of the reflected one ($|\tau|^2 = |r|^2$). This is the case for $I = -0.35$ Å. We will also neglect losses of the pulses due to magnetic damping on their way to and from the barrier, thus effectively moving the ports to the edges of the barrier. In addition, we will neglect the signal loss within the barrier due to the same magnetic damping. As the barrier is short, this loss is insignificant. Under these conditions and considering the energy conservation law ($|\tau|^2 + |r|^2 = 1$), we obtain $|S_{11}| = |S_{21}| = |S_{22}| = |S_{12}| = |\tau| = |r| = \frac{1}{\sqrt{2}}$.

We also need phases of these quantities. To find the phases, in Fig. 4, we plot the phase differences $\Delta\phi_1 = \arg(S_{21}) - \arg(S_{11})$ and $\Delta\phi_2 = \arg(S_{12}) - \arg(S_{22})$, where $\arg(z)$ denotes the phase of a complex number z. We obtain the phase differences from simulating single pulses incident to the barrier either from port 1 or 2. The data are shown for the case of the perfectly semitransparent BVMSW mirror ($I = -0.35$ A).
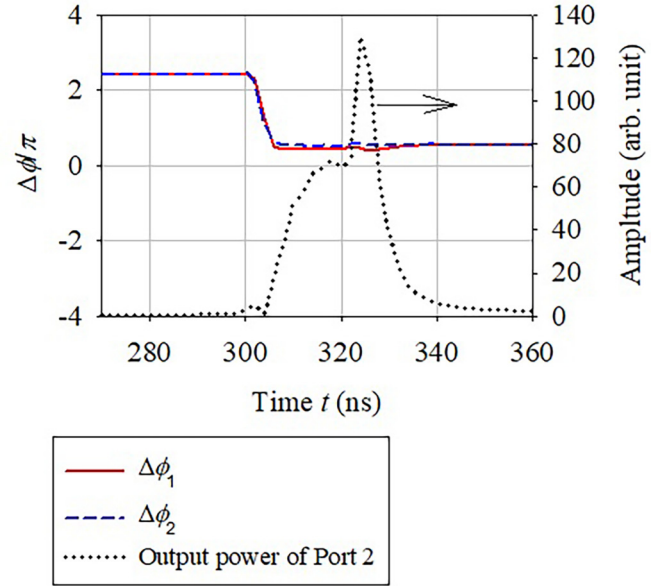

FIG. 4. Thick solid line: difference in phases $\Delta\phi_1$ of signals received by ports 1 and 2, when a single input pulse is applied to Port 1. Dashed line: the same, but the single input pulse is now applied to Port 2 ($\Delta\phi_2$). Dotted line: microwave output power of Port 2, when a single input pulse is applied to Port 1 (right-hand vertical axis). $I = -0.35$ A. The other simulation parameters are the same as for Fig. 2.

This is the configuration of Fig. 3(b). Calculating the differences eliminates phase accumulation by the signals on their paths to and from the barrier. Again, this approach is consistent with moving the ports to the edges of the barrier.

For convenience, we also show the simulated $|S_{21}|^2$ in the same graph. One sees that both phase differences are very close to $\pi/2$ within the pulses. This explains why phase differences of $\pm\pi/2$ between the input pulses switch the direction of the large-amplitude output pulse [Fig. 3(c)]. By adding or subtracting $\pi/2$ to or from either $\Delta\phi_1$ or $\Delta\phi_2$, we create conditions for constructive interference of scattered pulses incident to one port (*bright port* in the following) and for destructive interference for pulses traveling toward the other port (*dark port*). Changing the sign of this extra phase shift swaps the interference conditions for the ports and sends the large-amplitude pulse in the opposite direction of axis x with respect to the original one. (The dark port becomes bright and vice versa.)

We may assign the phase $\Delta\phi_1 = \Delta\phi_2 = \pi/2$ either to the diagonal (r) or antidiagonal (τ) elements of the matrix, as we are not interested in the absolute phase accumulation by the signal while being scattered from the barrier but just in the phase difference between the transmitted and reflected waves, given the reciprocal character of the mirror. Assigning the phases to the transmission coefficients yields a transfer matrix as follows:

$$\hat{S} = \frac{1}{\sqrt{2}} \begin{pmatrix} 1 & i \\ i & 1 \end{pmatrix}. \qquad (3)$$

The matrix has the same form as the transfer matrix for the symmetric beam splitter of Loudon [3,17]. This finding im-

plies that the formalism from Refs. [2,4] applies to our SW mirror. It allows calculating the output quantum state of the mirror for the case when single magnons are incident on ports 1 and 2.

Let us now discuss a potential SW HOME experiment. The experiment can be organized in a way like one from Ref. [4]. An electrically controlled qubit is connected to each SW transducer. The qubits release single microwave photons simultaneously. The transducers convert the primary photons into single magnons. The magnons propagate toward the barrier and interact there. The same transducers are used to convert the scattered magnons into secondary photons. The secondary photons are captured by the same qubits connected to the transducers. Employing the qubits as both photon sources and photon detectors is possible because of the presence of a delay time t_d in the system—it takes time t_d for the magnons to arrive to the transducers once they have been launched into the film and scattered from the barrier. The delay time $t_d = d/|V_g|$. For our example of the SW carrier wave number $k = 49$ rad/cm, $|V_g| = 2.2 \times 10^6$ cm/s. For $d = 7$ mm, we then obtain $t_d = 320$ ns, and for $d = 4$ mm, $t_d = 185$ ns. If the primary photons released by the qubits are shaped as 20-ns-long pulses, it will be ample time to prepare the qubits for capturing the secondary photons.

If two bosons arrive simultaneously to two detectors, they are called *coincidence bosons*. Consider coincidence magnons. These magnons must be fully indistinguishable. From Fig. 3(b), we clearly see that the output pulses of the mirror overlap in time quite well. Hence, coincident arrival of two single magnons, shaped as those pulses, to the two ports is possible, provided they have been excited simultaneously. Hence, in Figs. 3(b) and 3(c), we deal with coincidence magnons.

We assume that two single microwave photons are incident simultaneously on ports 1 and 2 to create two coincident initial magnons. We will denote this state $|1, 1\rangle_{in}$. The reflected and transmitted pulses from Fig. 3(b) have very similar shapes. Therefore, for simplicity, we may assume that the respective single-photon-state spectral amplitude functions [2,4] are identical. In addition, the pulses from Fig. 3(b) overlap very well in time. Therefore, it is reasonable to assume that the relative time delay of arrival of the pulses to the transducers [4] vanishes. Under these assumptions, the last equation from sec. A in the online supplemental material of Ref. [4] reduces to simple formulas from table 1 in Ref. [3].

As follows from the third cell of the third column of the table in Ref. [3], the probability P_{11} of the observation of single microwave photons simultaneously exiting both ports (the output state $|1, 1\rangle_{out}$) is given by

$$P_{11} = (|\tau|^2 - |r|^2)^2 = (1 - 2|r|^2)^2 = \frac{(1 - R^2)^2}{(1 + R^2)^2}, \quad (4)$$

where $R = |\tau/r|$. One sees that, for a perfectly semitransparent mirror ($|\tau|^2 = |r|^2 = \frac{1}{2}$), this formula reduces to $P_{11} = 0$. This implies that the output state of the system is either $|0, 2\rangle_{out}$ or $|2, 0\rangle_{out}$. Each of these states is characterized by the presence of both coincidence photons at the same port—either Port 2 or Port 1, respectively. The probabilities P_{02} and P_{20} to observe these states are given by the second and fourth cells of

the same column of the table. Both probabilities are the same and are equal to $2|\tau|^2|r|^2$, which reduces to $P_{02} = P_{20} = \frac{1}{2}$ for the semitransparent mirror.

Note that Eqs. (3) and (4) are valid for a lossless medium. Because of the very short length of the potential barrier, it is acceptable to neglect magnetic losses in the mirror. However, we cannot neglect propagation losses of a SW on its path from an input port to an output one. Our simulation for $I = 0$ shows that, for $d = 7$ mm, the BVMSW propagation losses are 18 dB, which makes 2.6 dB/mm. This signal attenuation does not include transducer impedance mismatch loss (see, e.g., Ref. [18]). In physical experiments, transducers are not usually well impedance matched. Therefore, we may expect 5–10 dB of loss of conversion of power of an input microwave signal into a SW signal by an input transducer. The same then applies to the back conversion by an output transducer. In addition, the input transducer will lose an extra 3 dB of energy for exciting a BVMSW pulse, which travels in the $-x$ direction. This loss is usually termed *bidirectionality loss*. The bidirectionality loss also takes place at the output transducer—only half of SW power incident to the output transducer contributes to generating the output microwave signal. Hence, the total insertion loss of our device is $18 \text{ dB} + (2 \times 10 \text{ dB}) + (2 \times 3 \text{ dB}) = 44 \text{ dB}$ if we use the conservative estimation of the transducer conversion losses of 10 dB per transducer. Note that we did not have to choose $d = 7$ mm. A smaller transducer separation of $d = 4$ mm usually works fine in SW experiments and technology. For $d = 4$ mm, we will have $(2.6 \times 4) \text{ dB} + (2 \times 10 \text{ dB}) + (2 \times 3 \text{ dB}) \approx 36 \text{ dB}$. This implies that, for $d = 4$ mm and $I = 0$, we will have $|\tau|^2 = 10^{-36/10} = 2.5 \times 10^{-4}$. Then from the energy conservation law, for a semitransparent mirror ($I = -0.35$ A), we must have $|\tau|^2 = |r|^2 = \frac{2.5 \times 10^{-4}}{2} = 1.25 \times 10^{-4}$.

In Ref. [19], it was shown that the formalism from Ref. [3] remains valid in the presence of losses in a medium, provided that τ and r remain orthogonal ($\tau = i r$) in the presence of a loss and we count coincidence output states only. As seen from Fig. 4, the condition $\tau = i r$ is satisfied for the semitransparent BVMSW mirror ($|\tau|^2 = |r|^2$). The theory from Ref. [19] shows that, for the input state $|1, 1\rangle_{in}$ and $|\tau|^2 = |r|^2$, two boson detectors never click simultaneously—either one of the detectors clicks and the other remains silent (noncoincident photon states $|1, 0\rangle_{out}$ and $|0, 1\rangle_{out}$), or one detector displays a signal of simultaneous arrival of two bosons, but the other detector remains silent (states $|0, 2\rangle_{out}$ or $|2, 0\rangle_{out}$).

Equation (3.12) from [19] expresses probabilities of observing the output states of a lossy mirror. Specifically for the perfectly semitransparent lossy magnon mirror ($I = -0.35$ A), $\tau = i r$, and complete temporal overlap of output pulses [Fig. 3(b)], the probability of one quasiparticle to survive $P_{10} = P_{01} \approx 2|r|^2 = 2 \times 1.25 \times 10^{-4} = 2.5 \times 10^{-4}$. The probability of observing no microwave photon at either port (the output state $|0, 0\rangle_{out}$) $P_{00} = (1 - 2|r|^2)^2 \approx 1$. Similarly, the probabilities to observe one microwave photon at each port $P_{11} = 0$ and for both photons to exit the same port are $P_{02} = P_{20} = 2|r|^4 = 3.1 \times 10^{-8}$.

Assume that we can apply single microwave photons to the device with a repetition period of 10 μs. Then we may expect

one detection of either state $|0, 2\rangle_{out}$ or $|2, 0\rangle_{out}$ every 300 s or so. This will allow us to collect reliable statistics within a couple of hours of running the experiment.

Note that we need to count coincidence photons only (we will call this *coincidence events* in the following) and ignore all $|1, 0\rangle_{out}$ and $|0, 1\rangle_{out}$ states. However, while acting as microwave photon detectors, some types of qubits may be able to absorb just one microwave photon and unable to absorb two photons [4]. Therefore, in this earlier work, the experimentalists had to rely on an indirect method of observing the $|0, 2\rangle_{out}$ and $|2, 0\rangle_{out}$ states. They counted the $|1, 1\rangle_{out}$ states as a function of the degree of indistinguishability of the single photons and saw that this dependence has a sharp minimum for the highest degree of phonon indistinguishability. We believe that the same method can also be used for the BVMSW magnons. Furthermore, one can use the same way of controlling magnon distinguishability—by delaying the launch of one of the single magnons into the film. One expects to see a minimum in the number of $|1, 1\rangle_{out}$ coincidence events for vanishing time delay. The observation of the drop in P_{11} will evidence that $|2, 0\rangle_{out}$ and $|0, 2\rangle_{out}$ states are created instead of $|1, 1\rangle_{out}$ states.

Alternatively, one may exploit the electric control of transparency of the SW mirror, which is unique for SWs. Set I to 0 first and measure the P_{11} and $P_{10} + P_{01}$. Then turn on I, set the mirror transparency to 50% by properly adjusting the current, and repeat the experiment. Observation of a decrease in $P_{11}/(P_{10} + P_{01})$ will then evidence the presence of the magnonic HOME. (Because magnetic damping in the barrier may be different from elsewhere, it may be worth normalizing P_{11} by $P_{10} + P_{01}$, as we did in the formula above, to account for the small potential change in the overall level of magnetic losses in the presence of the barrier.)

It may also be worth measuring P_{11} as a function of I. Figure 5(b) shows the $P_{11}(I)$ dependence calculated with Eq. (4) using the values of $R(I)$ from Fig. 5(a) and assuming that the phase difference between τ and r is $\pi/2$ for any I. We checked the latter assumption with numerical simulations for a range of I values from -1 to -0.1 Å. We found that it is satisfied with good accuracy over the whole range. The graph in Fig. 5(b) is characterized by three zeros of $P_{11}(I)$ corresponding to three I values, for which $R(I) = 1$ [see Fig. 5(a)]. Observation of the zeros (or potentially just minima in a real-life experiment) will also evidence the presence of a magnonic HOME.

It is worth explaining why we propose using the tunneling regime ($I < 0$) of the BVMSW interaction with the energy barrier for creating the semitransparent mirror. Our simulations show that, in this regime, the shape of SW pulses changes less during the process of scattering from the barrier. As seen in fig. 4 from Ref. [11], the k dependence of the efficiency of scattering of a CW SW signal from the barrier is more significant for the scattering regime ($I > 0$); therefore, the larger pulse shape distortion is expected for $I > 0$. Our modeling shows that, for $I > 0$, the shapes of the transmitted and reflected pulses differ more significantly than for $I < 0$. This results in a weaker suppression of the SW pulse traveling to the dark port [Port 2 for $\phi = -\pi/2$ in notations of Fig. 3(c)], which is a signature of larger distinguishability of the interacting single magnons. Then the approximation
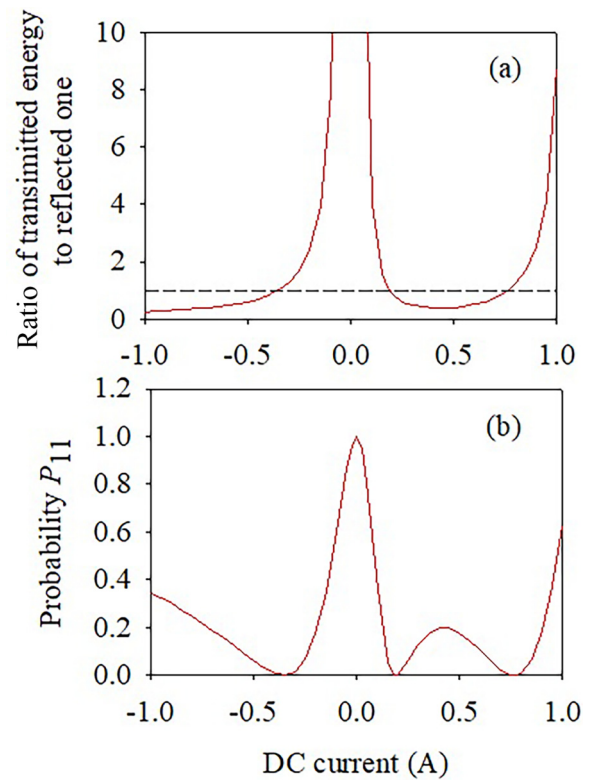

FIG. 5. (a) Ratio R of energy of the pulse received by Port 2 to energy of the pulse received by Port 1 as a function of the current I creating the potential barrier. The input microwave pulse is applied to Port 1. (b) Probability to observe the quantum state $|1, 1\rangle_{out}$ if the input quantum state of the device is $|1, 1\rangle_{in}$ as a function of I.

of the perfect indistinguishability of the incident magnons is less justified for $I > 0$, and the full HOME theory in the appendix from Ref. [4] needs to be employed for evaluating the efficiency of HOME for $I > 0$. This is beyond the scope of this paper. Here, we only mention that, due to this effect, we may expect less perfect zeros of P_{11} for $I > 0$ than shown in Fig. 5.

One more technical aspect of the proposed experiment needs to be addressed. Like Ref. [4], the device needs to be cooled down to millikelvin temperatures to suppress thermal magnon noise and thus create a noise floor which is low enough for observation of single traveling magnons. There should be no significant difference between thermal phonons from Ref. [4] and thermal magnons in YIG films in this regard. Therefore, the successful excitation of single phonons by releasing single microwave photons from superconducting qubits and detection of the phonons with the qubits is a good indicator that this process will potentially work for single magnons too. In fig. S1(b) in appendix 1.4 from Ref. [4], one sees that the transmission loss of the SAW device is 22 dB or so, despite careful optimization of the transducers. If properly optimized, the transmission loss of a SW device can be as low as 5 dB [20]. For BVMSWs, we need to add 6 dB of the antenna nondirectionality loss to this value, which makes 11 dB in total. Above, we assumed unoptimized BVMSW transducers, as typical for physical experiments, which yielded 36 dB of transmission loss. Despite this, our

estimation above shows that detecting coincidence magnons with a qubit will be possible within a realistic timeframe for the observation.

Conversely, if through some effort of transducer optimization, 5 dB of transduction losses per antenna are achieved (which is still significantly larger than the benchmark result from Ref. [20]), together with the 6 dB of the bidirectionality loss and 10 dB of the SW attenuation over the distance of 4 mm, this will make 26 dB of total transmission loss. This value is equivalent to just 1.5 times smaller transmitted power than in Ref. [4] ($26-22\,\text{dB} = 4\,\text{dB} = 1.5\,\text{times}$). This negligible difference suggests a good chance to observe the HOME for BVMSW magnons experimentally.

One important technical issue specific to traveling magnons in YIG films must be resolved to make the experiment possible though. Single-crystal YIG films are usually grown epitaxially on gadolinium gallium garnet (GGG) substrates. Unfortunately, GGG becomes paramagnetic at cryogenic temperatures. This increases SW propagation loss significantly [12]. However, as follows from literature, the substrate can be etched away locally to form a suspended bridge from a YIG film [21]. This may be a potential solution to this problem. Perhaps one can even etch the whole substrate away after fixing the other surface of the film to a solid diamagnetic slab having a similar thermal expansion coefficient. An alternative solution to this problem may be using a substrate-free YIG layer obtained by polishing down a thick single-crystal YIG slab [6].

IV. CONCLUSIONS

Through numerical simulations employing an original formalism, we demonstrated that a potential barrier for magnons, created by an Orsted field of a dc current flowing through a wire sitting on top of a YIG film, can act as an electrically controlled partly transparent mirror for the magnons. We considered the BVMSW configuration specifically and found that the mirror transparency can be set to 50% ($R = 0.5$) by properly adjusting the current strength, thus creating a semitransparent mirror. The strongest HOME is expected for single magnons in the $R = 0.5$ configuration. The effect must be seen as both coincidence magnons, launched into the film from two transducers (ports) located from the opposite sides of the mirror, simultaneously arriving to the same transducer and creating a two-microwave-photon state at the transducer output port. The probabilities of seeing those two-photon states at either output port must be the same. This result applies to coincidence magnons only. Due to significant transmission loss of the device, most of detection events will be detecting no output photons.

APPENDIX A: DERIVATION OF EQ. (1)

Following the idea from Ref. [11], we may write

$$\chi^{-1}(\omega)\tilde{m}(x,\omega) = \int_{-\infty}^{\infty} \hat{G}(x-x')\tilde{m}(x',\omega)dx' + \delta h(I,x) + \tilde{h}_{\text{dr}}(x,\omega), \quad \text{(A1)}$$

where

$$\chi(\omega) = \frac{\omega_H \omega_M}{\omega_H^2 - \omega^2}, \quad \text{(A2)}$$

and $\chi^{-1}(\omega) = (\omega_H^2 - \omega^2)/(\omega_H \omega_M)$ accordingly, $\omega_H = \gamma(H + i\Delta H)$, H is a spatially homogeneous applied field, i is imaginary unit, $\omega_M = \gamma\mu_0 M$, μ_0 is permeability of vacuum, M is the saturation magnetization of the films, γ is gyromagnetic ratio, $\delta h(I,x)$ is a spatially localized Oersted field of a wire that acts as a potential barrier for SWs, I is a dc current through the wire that creates the Oersted field, and $\tilde{m}(x,\omega)$ and $\tilde{h}_{\text{dr}}(x,\omega)$ are the perpendicular-to-film-plane vector components of the dynamic magnetization of BVMSWs and of the microwave driving field, respectively. Both have been averaged over the film thickness L and are assumed to be oscillating at a microwave frequency ω. To account for magnetic losses in the YIG film, we add an imaginary part $i\Delta H$ to the applied field H while calculating the parameter ω_H [22]. Here, ΔH is the magnetic loss parameter of the material.

Here, $\hat{G}$ is the Green's function of the perpendicular-to-plane dipole field of dynamic magnetization [15] averaged over the film thickness L:

$$\hat{G}(s) = \frac{2}{L} \ln\left[\frac{s^2}{s^2 + L^2}\right], \quad \text{(A3)}$$

where s is a dummy variable.

We now perform an inverse Fourier transform of both sides of Eq. (A1) with respect to ω. We obtain

$$\int_{-\infty}^{\infty} \exp(i\omega t)\tilde{h}_{\text{dr}}(x,\omega)d\omega = \tilde{h}_{\text{dr}}(x,t),$$

and

$$-\int_{-\infty}^{\infty} \omega^2 \exp(i\omega t)\tilde{m}(x,\omega)d\omega = \frac{\partial^2 \tilde{m}(x,t)}{\partial t^2},$$

where t is time. We then assume $\tilde{h}_{\text{dr}}(x,t) = h_{\text{dr}}(x,t)\exp(i\omega_0 t)$, where $h_{\text{dr}}(x,t)$ is a slow envelope of the waveform of the driving field $\tilde{h}_{\text{dr}}(x,\omega)$, and ω_0 is its microwave carrier frequency. Given the form of the driving term, we assume a similar solution for the dynamic magnetization: $\tilde{m}(x,t) = m(x,t)\exp(i\omega_o t)$, where $m(x,t)$ is a slow envelope of the waveform of $\tilde{m}(x,\omega)$. Upon substituting this solution into the Fourier transformed Eq. (A1) and ignoring an emerging $\partial^2 m(x,t)/\partial t^2$ term as negligibly small with respect to $\omega_0^2 m(x,t)$, which also appears in the equation, we obtain Eq. (1). In addition, while writing down Eq. (1), we consider that $h_{\text{dr}}(x,t)$ and $\delta h(I,x)$ are highly localized and do not overlap spatially.

APPENDIX B: EQUATION FOR $\delta h(i,x)$

We assume that the barrier $\delta h(I,x)$ is created by the Oersted field of a wire with a circular cross-section of a radius r. The wire lies directly on the surface of the YIG film. We are interested in the component of the Oersted field that is in the plane of the film. Employing Ampere circuital law and averaging the so-obtained in-plane component of the Oersted field over the film thickness, we obtain

$$\delta h(I,x) = \frac{1}{4\pi L} \ln\left[\frac{x^2 + (r+L)^2}{x^2 + r^2}\right]. \quad \text{(B1)}$$

APPENDIX C: SIMULATING MAGNON EXCITATION AND DETECTION BY THE WIRE-LOOP TRANSDUCERS

BVMSWs couple to the perpendicular-to-plane component of the microwave driving field. From the computational point of view, it is more convenient to assume wire-loop transducers in the form of one period of a meander line. This creates a current loop. (In a real-world experiment, simpler single-microstrip transducers will potentially be more convenient.) The advantage of the wire-loop transducers for the simulations is that the perpendicular component of their Oersted field is symmetric with respect to the symmetry axis of the transducer and strongly localized within the current loop. The focus of this paper is not on BVMSW excitation and detection. Therefore, for simplicity, we may assume that the driving field h_{dr} is uniform within the current loop (i.e., from $x = 0 - w_a/2$ to $0 + w_a/2$, where w_a is the width of the loop in the direction x) and vanishes elsewhere. The same applies to the second transducer located at $x = 7$ mm.

The same transducers may be used to receive the BVMSW signals. The operation of a receiving transducer is based on Faraday induction (see, e.g., Ref. [18]). Therefore, the output microwave voltage of the transducer must scale as microwave magnetic flux through the loop of the transducer. A good proxy for the latter is the BVMSW amplitude $m(x, t)$ integrated over the width of the loop w_a. The output power of the transducer then scales as the square of the flux and hence as the modulus square of the integral of $m(x, t)$ over the transducer loop width. We use the latter quantity as a proxy to output microwave power of the transducers. Energy of the output pulse is then obtained by integrating the output microwave power over the temporal width of the output pulse.

APPENDIX D: DEPENDENCE OF THE RATIO OF TRANSMITTED ENERGY TO REFLECTED ENERGY

The dependence of the ratio of transmitted energy to reflected energy $R(I)$ is obtained by solving Eq. (1) numerically, specifically for 20-nm-long microwave input pulses. It is displayed in Fig. 5(a). The graph shows R as the ratio of energies of pulses received by the respective ports. The dashed line in the figure shows the level of $R = 1$. Figure 5(b) displays the respective probability P_{11} to observe coincident single photons exiting ports 1 and 2 simultaneously (state $|1, 1\rangle_{out}$) as a function of I, when the input state of the device is $|1, 1\rangle_{in}$. The three points, where P_{11} vanishes, correspond to $R = 1$. To produce this graph, we used Eq. (4).

[1] C. K. Hong, Z. Y. Ou, and L. Mandel, Phys. Rev. Lett. **59**, 2044 (1987).

[2] A. M. Brańczyk, arXiv:1711.00080 (2017).

[3] H. Fearn and R. Loudon, Opt. Comm. **64**, 485 (1987).

[4] H. Qiao, E. Dumur, G. Andersson, H. Yan, M.-H. Chou, J. Grebel, C. R. Conner, Y. J. Joshi, J. M. Miller, R. G. Povey *et al.*, Science **380**, 1030 (2023).

[5] H. Y. Yuan, Y. Cao, A. Kamra, R. A. Duine, and P. Yan, Phys. Rep. **965**, 1 (2022).

[6] S. Kosen, A. F. van Loo, D. A. Bozhko, L. Mihalcean, and A. D. Karenowska, APL Mater. **7**, 101120 (2019).

[7] S. Knauer, K. Davidkova, D. Schmoll, R. O. Serha, A. Voronov, Q. Wang, R. Verba, O. V. Dobrovolskiy, M. Lindner, T. Reimann *et al.*, J. Appl. Phys. **133**, 143905 (2023).

[8] M. Kostylev and A. A. Stashkevich, J. Mag. Mag. Mat. **484**, 329 (2019).

[9] M. Kostylev, A. B. Ustinov, A. V. Drozdovskii, B. A. Kalinikos, and E. Ivanov, Phys. Rev. B **100**, 020401(R) (2019).

[10] S. O. Demokritov, A. A. Serga, A. Andre, V. E. Demidov, M. P. Kostylev, B. Hillebrands, and A. N. Slavin, Phys. Rev. Lett. **93**, 047201 (2004).

[11] M. P. Kostylev, A. A. Serga, T. Schneider, T. Neumann, B. Leven, B. Hillebrands, and R. L. Stamps, Phys. Rev. B **76**, 184419 (2007).

[12] R. W. Damon and J. R. Eshbach, J. Phys. Chem. Solids **19**, 308 (1961).

[13] R. W. Damon and H. Vandevaa, J. Appl. Phys. **36**, 3453 (1965).

[14] M. Chen, M. A. Tsankov, J. M. Nash, and C. E. Patton, Phys. Rev. B **49**, 12773 (1994).

[15] K. Y. Guslienko and A. N. Slavin, J. Mag. Mag. Mat. **323**, 2418 (2011).

[16] A. K. Zvezdin and A. F. Popkov, Sov. Phys. JETP **57**, 350 (1983).

[17] https://en.wikipedia.org/wiki/Beam_splitter.

[18] C. Weiss, M. Bailleul, and M. Kostylev, J. Mag. Mag. Mat. **565**, 170103 (2023).

[19] S. M. Barnett, J. Jeffers, A. Gatti, and R. Loudon, Phys. Rev. A **57**, 2134 (1998).

[20] A. B. Ustinov, A. A. Nikitin, V. V. Lebedev, A. A. Serebrennikov, A. V. Shamray, A. V. Kondrashov, and B. A. Kalinikos, J. Phys. Conf. Ser. **1038**, 012033 (2018).

[21] F. Heyroth, C. Hauser, P. Trempler, P. Geyer, F. Syrowatka, R. Dreyer, S. G. Ebbinghaus, G. Woltersdorf, and G. Schmidt, Phys. Rev. Appl. **12**, 054031 (2019).

[22] A. G. Gurevich and G. A. Melkov, *Magnetization Oscillations and Waves* (CRS Press, London, 1996).